Influence of cerium substitution on boron doped $Zn_{0.5}Ca_{0.25}Cu_{0.25}Fe_{1.97}B_{0.03-y}Ce_yO_4$ ferrites for high-frequency applications

Z. Munir [a], M. I. Arshad [a], K.A. ElAziz [b], M. S. Al-Buriahi [c], N. Amin [a], H. T. Ali [b], K. Mehmood [a], M. Akhtar [a,d], M. Q. A. Malik [d], M. A. Gadhi [e], Iqra [a,*]
[a] *Magnetic & Innovative Materials in Nanotechnology (MiMi Nanotech) Research Lab, Department of Physics, Government College University, Faisalabad, Pakistan 38000*
[b] *Department of Mechanical Engineering , College of Engineering, Taif University, Kingdom of Saudi Arabia*
[c] *Department of Physics, Sakarya University, Sakarya, Turkey*
[d] *Centre for High Energy Physics, University of the Punjab, Lahore*
[e] *Head Medical Physics Department Atomic Energy Cancer Hospital-GINUM Gujranwala*

The increasing demand for high-performance materials in electronic and magnetic applications has highlighted the need to increase the structural, magnetic, and dielectric characteristics of ferrite materials. To address this, cerium substitution has been explored as an effective strategy for improving the properties of boron-doped ferrites. In this study, we investigate the influence of cerium (Ce) substitution on the structural, magnetic, and dielectric properties of $Zn_{0.5}Ca_{0.25}Cu_{0.25}Fe_{1.97}B_{0.03-y}Ce_yO_4$ ferrites. Characterization techniques, including Raman spectroscopy, IV measurements, dielectric testing, and vibrating sample magnetometry (VSM), were used to assess the effects of Ce substitution on the material's performance. Our results reveal significant improvements in dielectric and magnetic behavior, with Ce substitution offering enhanced stability across frequencies and temperatures. The findings highlight that these Ce-doped ferrites show promise for future high-frequency applications.

(Received August 4, 2025; Accepted November 4, 2025)

Keywords: Sol-gel auto combustion, Crystalline size, Bandgap, Resistivity

1. Introduction

The typical formula that is used for the spinel ferrites AB_2O_4 is created by the close-packed (FCC) arrangement of cations. The octahedral site includes divalent cations and the tetrahedral sites includes trivalent cations. The system is referred as normal when this arrangement of cations occurs [1]. The oxygen in spinel ferrites has the high electronegativity value that's why it attracts many electrons and forms ionic bonds. Due to the ionic bonds, the spinel structure formed has the closely packed anions [2]. The produced ferrite's properties are significantly affected by the arrangement of cations on the crystallographic regions [3]. This arrangement is determined by their chemical structure and the method used to synthesize them [4]. The preparation steps mainly processing and annealing temperature affects the grain size, grain border and crystallites size which determines the physical and chemical properties of the produced ferrites [5]. They have high resistivity value, low eddy current loses and microwave frequencies, so, spinel ferrites are helpful for many applications [6]. Boron spinel ferrites play a crucial role in various industries, finding applications in microwave technology and switching devices. Their unique inherited magnetic properties make them essential for reliable and efficient performance in these fields. By carefully substituting certain rare earth (RE) ions into the tiny gaps within a lattice, scientists can create materials with improved

* Corresponding author: iqraranaphysicst@gmail.com
https://doi.org/10.15251/JOR.2025.216.693

properties, making them more effective for specific applications [7]. Scientists have observed that adding rare earth (RE) elements causes noticeable changes in the material's structure. These RE elements influence the internal stresses and magnetic behavior of the ferrite, leading to modifications in its overall properties. Even a small amount of rare earth (RE) cations can significantly impact a material's structure and electromagnetic properties [8]. Studies have shown that adding elements like Ce, Er, or Dy to ferrites can noticeably alter their behavior and characteristics [9]. Today, many researchers are exploring how swapping one rare-earth element for another affects nano ferrites, aiming to understand the changes it brings to their properties [10]. Introducing Ce^{3+} into boron-doped $Zn_{0.5}Ca_{0.25}Cu_{0.25}Fe_{1.97}B_{0.03-y}Ce_yO_4$ enhances its magnetic imbalance, leading to spin frustration at low temperatures. Due to its redox reactivity, Ce-substituted materials are highly versatile and find a wide range of applications [11]. Solar cells, fuel cells, and oxygen storage devices are known to utilize Ce^{4+}–Ce^{3+} redox couples. Humidity sensors, on the other hand, often incorporate ceria-substituted boron ferrite due to its unique properties. However, there is a lack of comprehensive and systematic research specifically focused on cerium-substituted boron ferrites in the existing literature [15]. In this study, we synthesize nano-sized Ce^{3+}-substituted boron-doped $Zn_{0.5}Ca_{0.25}Cu_{0.25}Fe_{1.97}B_{0.03-y}Ce_yO_4$ (y = 0, 0.01, 0.02, 0.03) to explore the influence of cerium on the electrical, magnetic, and structural properties of boron ferrites. The materials are synthesized using the simple and cost-effective sol–gel auto-combustion process, which allows for efficient production and analysis of these characteristics.

2. Materials and methods

The The Ce^{3+}-substituted boron-doped $Zn_{0.5}Ca_{0.25}Cu_{0.25}Fe_{1.97}B_{0.03-y}Ce_yO_4$ ferrite samples were synthesized using the sol–gel auto-combustion technique due to its simplicity, cost-effectiveness, and ability to produce homogenous nano-sized powders. High-purity metal nitrates, including zinc nitrate ($Zn(NO_3)_2 \cdot 6H_2O$), calcium nitrate ($Ca(NO_3)_2 \cdot 4H_2O$), copper nitrate ($Cu(NO_3)_2 \cdot 3H_2O$), iron nitrate ($Fe(NO_3)_3 \cdot 9H_2O$), boron nitrate ($BB(NO_3)_2$), and cerium nitrate ($Ce(NO_3)_3 \cdot 6H_2O$), were used as starting precursors. Citric acid ($C_6H_8O_7$) served as the chelating agent.

Stoichiometric amounts of the metal nitrates and citric acid were dissolved in deionized water, ensuring a 1:1 molar ratio of total metal ions to citric acid. This mixture was then continuously stirred using a magnetic stirrer to achieve a homogeneous solution. Ammonia solution was carefully added dropwise to the mixture in order to adjust the pH to approximately 7, a crucial step in promoting the formation of the gel.

Following this, the mixture was heated at 80 °C under constant stirring to facilitate the gelation process, allowing the components to combine and form a consistent gel-like substance. This controlled process ensures the proper formation of the desired material for further synthesis.

Upon gel formation, the temperature was raised to approximately 370 °C to initiate the auto-combustion process. The gel underwent spontaneous combustion, yielding a voluminous ash-like product. This precursor was then calcined at 850 °C for 8 hours to improve crystallinity and eliminate residual organic matter. The resulting fluffy powder was ground thoroughly using an agate mortar to ensure homogeneity and reduce particle size, preparing the samples for further characterization.

Fig. 1. A schematic representation of the synthesis steps for the Ce^{3+}-substituted boron-doped $Zn_{0.5}Ca_{0.25}Cu_{0.25}Fe_{1.97}B_{0.03-y}Ce_yO_4$.

3. Results and discussions

Raman spectroscopy (Morphology 4-ID, 532.8 nm laser) was employed to identify vibrational modes and chemical bonding interactions within the material, providing insights into its structural properties. The electrical properties, including resistivity and conductivity, were measured using a Keithley 2401 Source Meter with a two-probe IV measurement system, offering accurate data on the material's response to applied voltage. Additionally, dielectric parameters such as dielectric constant, loss tangent, and AC conductivity were determined using an IM3533 LCR meter and Impedance Analyzer (IA) at room temperature. These measurements are crucial for understanding the material's behavior in various electronic applications, providing essential data on how it responds to alternating electric fields and its overall performance in devices that rely on its dielectric and conductive properties.

3.1. Raman spectroscopy

Raman spectroscopy was used to find the molecular vibrational modes of the cerium substituted boron doped $Zn_{0.5}Ca_{0.25}Cu_{0.25}Fe_{1.97}B_{0.03-y}Ce_yO_4$ ferrites. The Lorentz fit spectra for these soft ferrites ranged from 200-800 cm^{-1} [12].

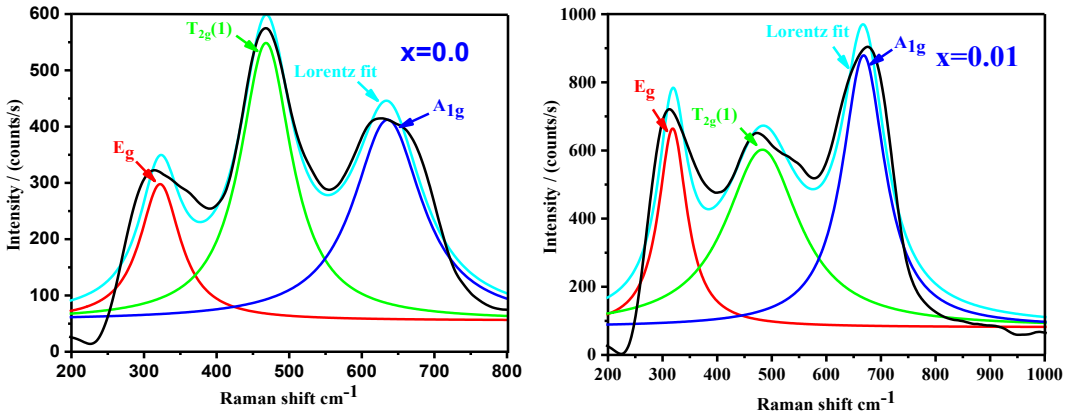

Fig. 2. Raman Spectroscopy results for cerium substituted boron doped $Zn_{0.5}Ca_{0.25}Cu_{0.25}Fe_{1.97}B_{0.03-y}Ce_yO_4$ ferrites at x=0.0, x=0.01.

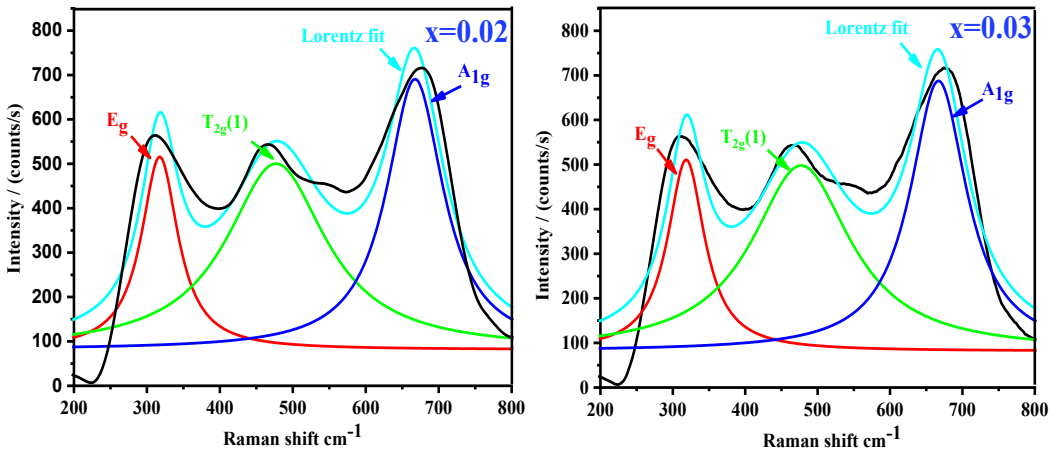

Fig. 3. Raman Spectroscopy results for cerium substituted boron doped $Zn_{0.5}Ca_{0.25}Cu_{0.25}Fe_{1.97}B_{0.03-y}Ce_yO_4$ ferrites at x=0.02, x=0.03

The Eg mode at the B-site explains about how oxygen ions vibrate around the octahedral cations [13]. Initially, its peak appears at 319.61 cm when x = 0 but as x increases to 0.02, the frequency gradually drops to 313.40 cm before slightly rising again at x = 0.03 This downward trend suggests that introducing cerium (Ce) into the structure distorts the lattice, altering the bond lengths and strengths at the B-site. The slight increase at x = 0.03 might indicate local strain effects or a stabilization of the structure [14]. The T2g mode at the A-site represents vibrations occurring in the tetrahedral structure due to interactions between metal and oxygen. The frequency shift fluctuates, initially increasing from 462.61 cm at x = 0 to 482.28 cm at x = 0.01 before decreasing at higher doping levels. This pattern suggests that cerium doping strengthens A-site metal-oxygen bonds at first but later disrupts the crystal structure, leading to disorder [15]. The Alg mode at the A-site is related to the symmetric stretching of oxygen in the tetrahedral sites. The Raman shift sees a sharp rise from 638.02 cm at x = 0 to 666.94 cm¹ at x = 0.01 followed by a slight increase at higher doping levels [16].

Table 1. Raman modes for the soft ferrites.

x	Raman shift (cm^{-1})		
	Eg (B-site)	T2g(1) (A-site)	A1g (A-site)
0	319.61	462.61	638.02
0.01	321.01	482.28	666.94
0.02	315.16	475.52	673.75
0.03	322.91	477.75	672.34

This significant increase at x = 0.01 suggests that Ce doping initially enhances interactions within the tetrahedral sites, likely due to a redistribution of cations between A- and B-sites. The Raman spectroscopy analysis shows how cerium (Ce) doping affects the lattice structure at both A- and B-sites, with distinct shifts in vibration modes, such as the Eg, T2g, and Alg. These changes suggest that Ce doping

can enhance or disrupt the material's crystal structure, which has implications for high-frequency applications where lattice stability and bond strength are critical for performance.

3.2. Current voltage analysis

Current-voltage (I-V) graphs were recorded for the Cerium substituted boron doped $Zn_{0.5}Ca_{0.25}Cu_{0.25}Fe_{1.97}B_{0.03-y}Ce_yO_4$ ferrites using a two-probe instrument with the Keithley I-V electrometer model 2401. The measurements were recorded within a temperature range of 313–623 K. (A) demonstrates the variations in DC resistivity of the prepared ferrites versus temperature. The resistivity values were calculated using the equation provided in reference [17], allowing for a detailed understanding of how the resistivity varies with temperature in these ferrite materials. These measurements help in understanding the electrical properties of the ferrites and their behavior under different temperature changing conditions, thus giving valuable understanding for potential applications in electronic devices and sensors.

$$\rho = \frac{RA}{L}$$

where ρ is the resistivity of the material, A and L shows the surface area and thickness of all pellets, respectively [18].

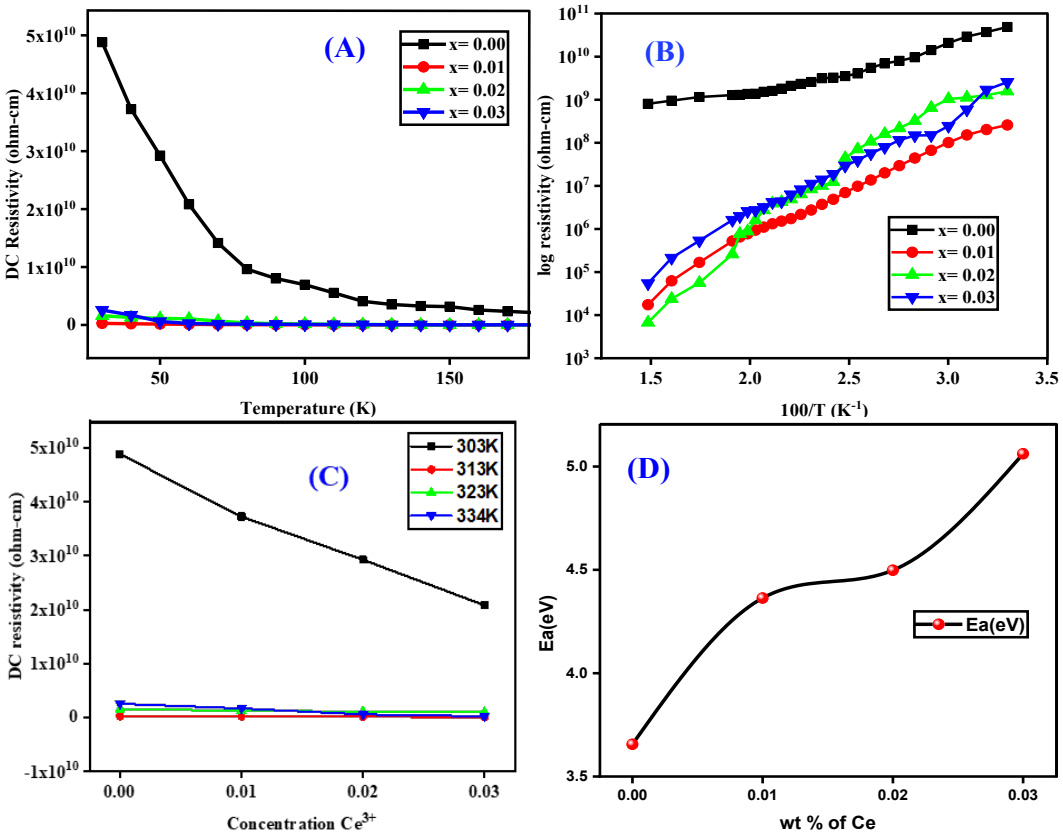

Fig. 4. (A) DC resistivity (Ω-m) vs variation of temperature, (B) log of resistivity (Ω-m) vs variation in (1000/temperature); (C) DC resistivity against temperature, (D) Activation energy vs. cerium concentration.

(A) shows that the resistivity of the undoped sample (y = 0.00) is extremely high compared to the Ce^{3+}-doped ones. As the temperature increases, the resistivity decreases for all compositions, which is typical behavior for semiconductors. Essentially, as the temperature rises, more charge carriers are excited, improving the material's ability to conduct electricity. However, what is particularly interesting here is that as cerium is added, the resistivity drops significantly. This suggests that cerium plays a crucial role in enhancing the material's conductivity, likely by introducing additional charge carriers, which is confirmed by earlier studies [18]. Furthermore, the maximum DC resistivity is observed in the x = 0.0 sample, confirming that this undoped sample is more suitable for transformer applications, where minimizing eddy current losses is important. The decreasing trend in DC resistivity can be attributed to the fact that Ce^{3+} has a lower electrical conductivity (1.4×10^6 $(Ohm.m)^{-1}$) compared to Fe^{3+} (9.9×10^6 $(Ohm.m)^{-1}$), which means the doping process reduces the overall resistivity.

Additionally, (B) illustrates the relationship between the logarithm of DC resistivity and 1000/T. The results reveal the semiconductor behavior of the synthesized nano ferrites. The undoped sample still exhibits the highest resistivity, while the doped ones show a clear reduction in resistivity with increasing temperature. The straight-line trend in the graph confirms that the conduction mechanism follows a thermally activated process, meaning heat facilitates the movement of electrons and charge carriers. This type of behavior is typical for ferrites, where the electrical transport is controlled by the hopping mechanism between ions, a key factor in understanding the material's conduction properties [19].

Figure (C) shows resistivity against cerium concentration at different temperatures, providing another key insight into the behavior of the material. At room temperature (303 K), the undoped material exhibits extremely high resistivity, indicating poor electrical conductivity. However, as cerium is introduced into the material, the resistivity drops significantly up to a cerium concentration of y = 0.02, after which the resistivity begins to level off. This suggests that there is an optimal cerium doping level that maximizes conductivity. Adding too much cerium, as seen at y = 0.03, could introduce defects or disrupt the crystal structure, which ultimately limits the material's ability to further improve its conductivity. This trend emphasizes the importance of finding the right balance in doping to achieve the best electrical properties. The activation energy also varies with cerium concentration, showing a marked increase up to a certain point before it decreases. At x = 0, the activation energy is approximately 0.2 eV, indicating relatively low resistance to charge carrier movement. As cerium concentration increases to 0.01, the activation energy rises to around 0.42 eV, reflecting a greater difficulty for charge carriers to move. The maximum activation energy, approximately 0.6 eV, is observed at x = 0.02, indicating the highest resistance to charge carrier movement [20]. However, when the cerium concentration increases further to 0.03, the activation energy slightly decreases to about 0.45 eV. This reduction suggests that, beyond a certain doping level, the material undergoes structural or electronic modifications that facilitate easier charge carrier movement, which in turn decreases the activation energy. The resistivity measurements highlight the significant impact of cerium (Ce) doping on the conductivity of the material, with a marked decrease in resistivity as cerium concentration increases, suggesting enhanced charge carrier availability. This behavior is critical for high-frequency applications, as it indicates improved electrical properties with optimized Ce doping, which could enhance performance in electronic devices where conductivity and efficient charge transport are essential.

3.3. Direct current analysis

The dielectric properties of boron-doped $Zn_{0.5}Ca_{0.25}Cu_{0.25}Fe_{1.97}B_{0.03-y}Ce_yO_4$ ferrites are significantly influenced by cerium (Ce) substitution, as evidenced in the presented graphs. The dielectric constant decreases with increasing frequency for all cerium concentrations, which is typical of many dielectric materials [21]. However, the rate of decrease is less pronounced at higher Ce concentrations, indicating that cerium substitution helps stabilize the dielectric constant at higher frequencies due to the accumulation of the electrons at the grain boundaries, hence the interchange of the electrons also decreases [22].

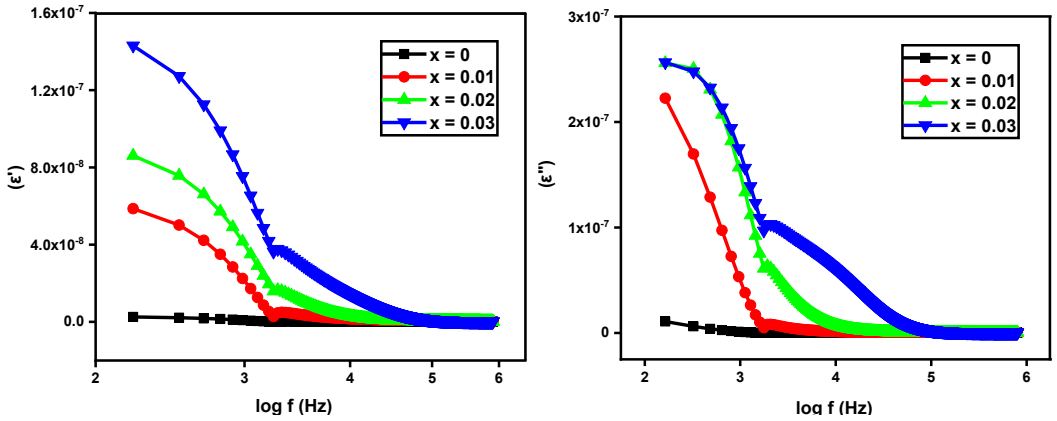

Fig. 5. (a) Log of frequency f (Hz) vs Real part of permittivity (b) log of f (Hz) vs Imaginary part of permittivity.

This stabilization is further supported by the behavior of the dielectric loss where energy loss decreases with increasing cerium content, and the change becomes steady at the higher frequency. [23].

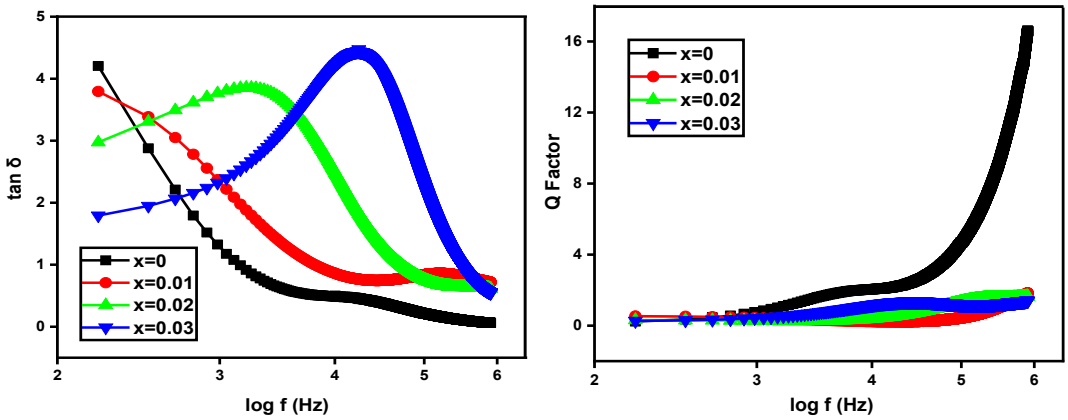

Fig. 6. (a) log of frequency f(Hz) dielectric tangent loss (b) log of frequency f(Hz) quality factor.

Additionally, the tangent loss follows a similar trend, with higher cerium concentrations resulting in lower losses at higher frequencies, making the material more efficient in energy storage and conversion. This is due to the wo layers the prepared samples contain. One includes grains and the other includes the grain boundaries. At higher frequency, less energy is required for the hopping of the Fe ions. The loss tangent, which measures energy dissipation as heat, becomes progressively lower with higher cerium substitution, demonstrating the improved efficiency of the material This made these nanocomposites suitable for many high-frequency microwave applications [24]. The quality factor Q is shown to increase with frequency, further emphasizing the stabilizing effect of Ce on the material's dielectric properties [25]. The impedance exhibits a reverse trend with the increase in frequency explained by the Maxwell-Wagner model [26]. These trends confirm that cerium substitution enhances the material's performance by minimizing energy dissipation and improving the material's efficiency, particularly at higher frequencies. This makes the material more suitable for high-frequency applications, where both stable dielectric properties and low energy loss are crucial.

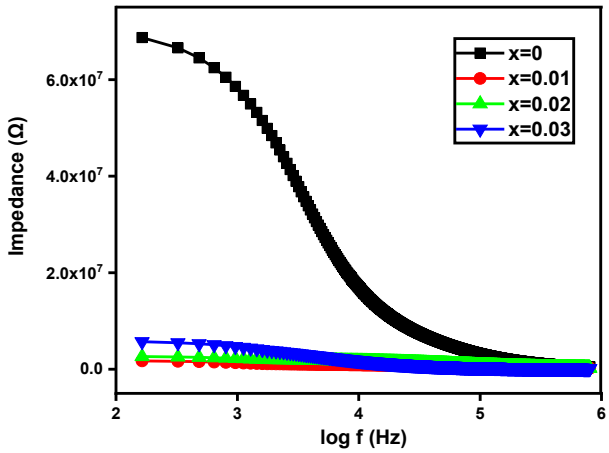

Fig. 7. lof of frequency f(Hz) vs Impedance.

Cerium (Ce) substitution in boron-doped $Zn_{0.5}Ca_{0.25}Cu_{0.25}Fe_{1.97}B_{0.03-y}Ce_yO_4$ ferrites stabilizes the dielectric constant and reduces energy loss, making the material more efficient for high-frequency applications. At higher Ce concentrations, the decreased dielectric loss and lower tangent loss enhance the material's performance, making it ideal for energy storage and conversion in microwave and high-frequency electronic devices.

3.4. Hysteresis Loop Analysis

Vibrating Sample Magnetometer (VSM) instrument was used to measure and calculate the magnetic properties of the samples. Fig. 8 displays the M-H hysteresis loop for $Zn_{0.5}Ca_{0.25}Cu_{0.25}Fe_{1.97}B_{0.03-y}Ce_yO_4$ ferrite with various Ce^{3+} ion concentrations, denoted by y = 0, 0.01, 0.02, recorded at room temperature. Magnetic characteristics such as saturation magnetization, remanent magnetization, coercivity, and squareness ratio (SQ) were determined using the VSM data, with the findings shown in Table 2. Table 2 indicates that an increase in cerium ion concentration results in a decrease in the values of the magnetic parameters. When the magnetization gets decreased, the number of holes within the material gets increased due to reduction in the recombination process, which reduces the magnetization of material in the given volume and interferes with electron transfer between grains [27].

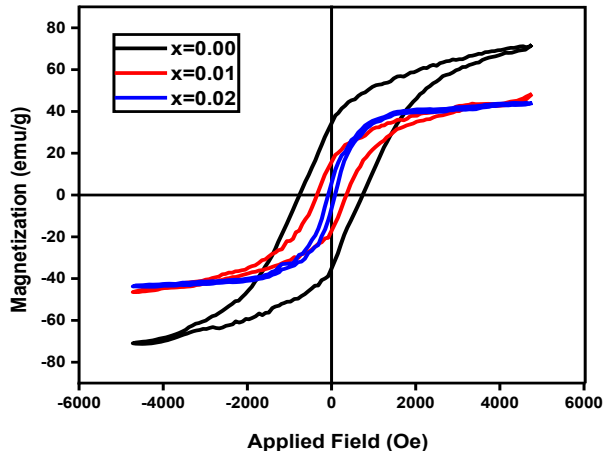

Fig. 8. Hysteresis loops for Ce^{3+}.substituted B Doped $Zn_{0.5}Ca_{0.25}Cu_{0.25}Fe_{1.97}B_{0.03}-yCe_yO_4$ Ferrites.

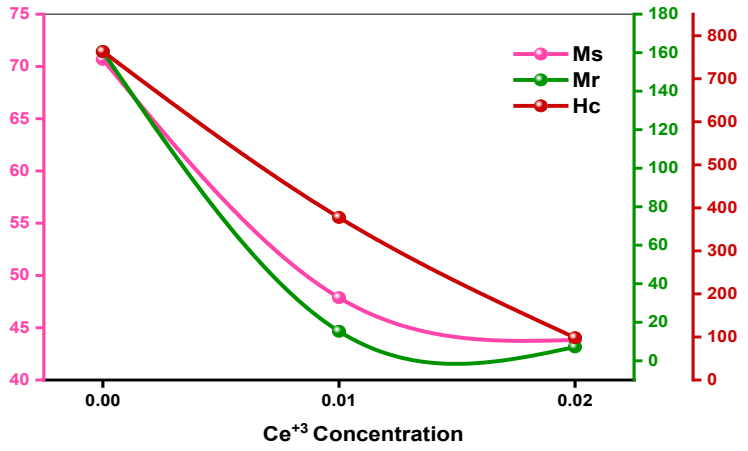

Fig. 9. Ms, Mr, and Hc values for Ce^{3+}.substituted B Doped $Zn_{0.5}Ca_{0.25}Cu_{0.25}Fe_{1.97}B_{0.03-y}Ce_yO_4$ Ferrites.

The magneto-crystalline anisotropy constant (K = Hc × Ms / 0.96) was evaluated and is clearly presented in Table 2. As the cerium ion concentration increases, the coercivity decreases from 763.33 Oe to 98.45 Oe, which can be attributed to the reduction in the anisotropy field, leading to a lower domain wall energy. Additionally, a decrease in the squareness ratio (Mr/Ms) with increasing Ce content was observed, indicating that the synthesized samples exhibit multi-domain magnetic behavior. This characteristic is important for achieving soft magnetic properties, making them suitable for applications in high-frequency transformers, motors, inductors, and generators [28]. Another factor that may contribute to the reduction in magnetization is the decrease in particle size [29].

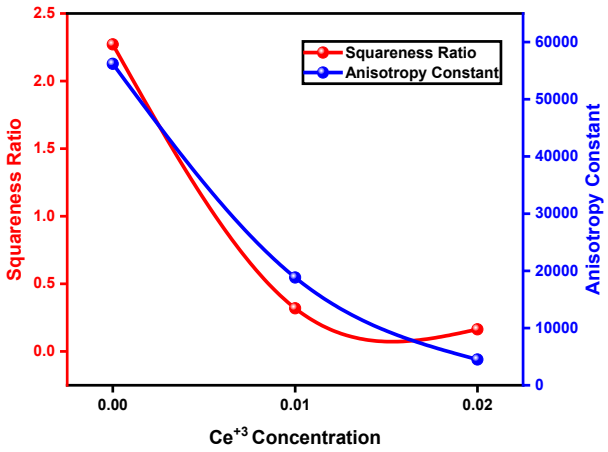

Fig. 11. Anisotropy Constant and Squareness ratio for Ce^{3+}.substituted B Doped $Zn_{0.5}Ca_{0.25}Cu_{0.25}Fe_{1.97}B_{0.03-y}Ce_yO_4$ Ferrites.

Table 2. Magnetic Parameters for Ce^{3+}.substituted B Doped $Zn_{0.5}Ca_{0.25}Cu_{0.25}Fe_{1.97}B_{0.03-y}Ce_yO_4$ Ferrites.

X	H_C (Oe)	M_r (emu/g)	M_s (emu/g)	SQ	K (erg/cm^3)
0.00	763.33	160.5	70.67	2.27112	56192.2199
0.01	377.56	15.28	47.88	0.31913	18830.805
0.02	98.49	7.16	43.84	0.16332	4497.71

The increase in cerium (Ce) ion concentration in $Zn_{0.5}Ca_{0.25}Cu_{0.25}Fe_{1.97}Ba_{0.3-y}Ce_yO_4$ ferrites leads to a decrease in magnetic parameters such as saturation magnetization, coercivity, and squareness ratio, resulting in soft magnetic properties. This reduction in coercivity and magnetization, along with the decrease in particle size, makes these materials suitable for high-frequency applications like transformers, motors, and inductors, where low coercivity and soft magnetic behavior are essential for efficiency.

4. Conclusion

In conclusion, the study demonstrates that cerium substitution significantly influences the structural, magnetic, and dielectric properties of boron-doped $Zn_{0.5}Ca_{0.25}Cu_{0.25}Fe_{1.97}B_{0.03-y}Ce_yO_4$ ferrites. The characterization results, including Raman spectroscopy, IV measurements, dielectric testing, and vibrating sample magnetometry (VSM), highlight the enhanced performance of the material with increasing cerium content. Specifically, cerium substitution improves the dielectric constant and reduces energy loss, making the material more efficient at high frequencies. The magnetic properties also showed significant improvements, suggesting potential applications in advanced electronic and magnetic devices. Future work will focus on optimizing the cerium concentration and exploring other dopants to further enhance the material's properties. This research lays the foundation for developing high-performance ferrite materials with wide-ranging applications in the fields of electronics and magnetics.

Acknowledgments

The authors would like to acknowledge Deanship of Graduate Studies and Scientific Research, Taif University for funding this work.

References

[1] S. Aman, N. Ahmad, B.S. Almutairi et al., J. Electron. Mater. 52, 4149-4161 (2023); https://doi.org/10.1007/s11664-023-10396-9

[2] R.J. Hill, J.R. Craig, G.V. Gibbs, Phys. Chem. Miner. 4(4), 317-339 (1979); https://doi.org/10.1007/BF00307535

[3] K. Pubby, K.V. Babu, S.B. Narang, Mater. Sci. Eng. B 255, 114513 (2020); https://doi.org/10.1016/j.mseb.2020.114513

[4] H.A. Alburaih, S.A. Khan, R.Y. Khosa et al., J. Korean Ceram. Soc. 60, 357-363 (2023); https://doi.org/10.1007/s43207-022-00270-5

[5] A. Toghan, M. Khairy, E.M. Kamar, M.A. Mousa, J. Market. Res. 19, 3521-3535 (2022); https://doi.org/10.1016/j.jmrt.2022.06.095

[6] F.F. Alharbi, S. Aman, N. Ahmad et al., J. Mater. Sci. Mater. Electron. 33, 12147-12156 (2022); https://doi.org/10.1007/s10854-022-08175-z

[7] M.S. Shah, K. Ali, I. Ali, A. Mahmood, S.M. Ramay, M.T. Farid, Mater. Res. Bull. 98, 77-82 (2018); https://doi.org/10.1016/j.materresbull.2017.09.063

[8] Z. Karimi, Y. Mohammadifar, H. Shokrollahi, S.K. Asl, G. Yousefi, L. Karimi, J. Magn. Magn. Mater. 361, 150-156 (2014); https://doi.org/10.1016/j.jmmm.2014.01.016

[9] M.A. Khan, M.U. Islam, M. Ishaque, I.Z. Rahman, Ceram. Int. 37(7), 2519-2526 (2011); https://doi.org/10.1016/j.ceramint.2011.03.063

[10] D. Chen, Y. Zhang, C. Tu, Mater. Lett. 82, 10-12 (2012); https://doi.org/10.1016/j.matlet.2012.05.034

[11] V. Šepelák, D. Baabe, D. Mienert, F.J. Litterst, K.D. Becker, Scr. Mater. 48(7), 961-966 (2003); https://doi.org/10.1016/S1359-6462(02)00600-0

[12] Nabi M, Moin M, Hasan M, Arshad M, Bibi A, Amin N, et al., J Supercond Nov Magnetism. 2021;34(7):1813; https://doi.org/10.1007/s10948-020-05588-x

[13] Graves P, Johnston C, Campaniello J., Mater Res Bull. 1988;23(11):1651; https://doi.org/10.1016/0025-5408(88)90255-3

[14] Datt G, Bishwas MS, Raja MM, Abhyankar A., Nanoscale. 2016;8(9):5200; https://doi.org/10.1039/C5NR06791J

[15] Amin N, Hasan MSU, Majeed Z, Latif Z, un Nabi MA, Mahmood K, et al., Ceram Int. 2020;46(13): 20798; https://doi.org/10.1016/j.ceramint.2020.05.079

[16] Rezlescu E, Sachelarie L, Popa P, Rezlescu N., IEEE Trans Magn. 2000;36(6):3962; https://doi.org/10.1109/20.914348

[17] N. Amin, R. Bilal, G. Mustafa, A. Aslam, M. Hasan, K. Hussain, M. Tabassum, M. Fatima, Z. Khan, A. Naseem, Dig. J. Nanomater. Biostruct. 14 (2019) 501-507.

[18] M. Arshad, M. Hasan, A.U. Rehman, N. Amin, N.K. Thanh, N. Morley, M. Amami, F. Alresheedi, S. Ezzine, M. Gadhi, J. Alloys Compd. 972 (2024) 172847; https://doi.org/10.1016/j.jallcom.2023.172847

[19] M. Akhtar, M. Hasan, N. Amin, N. Morley, M.I. Arshad, J. Rare Earths 42 (2024) 137; https://doi.org/10.1016/j.jre.2023.01.021

[20] A. Mujtaba, M. Khan, M. Hasan, S. Ali, W. Shahid, M. Fatima, H.S. Abd-Rabboh, N. Alwadai, J. Mater. Res. Technol. 23 (2023) 4538; https://doi.org/10.1016/j.jmrt.2023.02.038

[21] Malana, M.A., Qureshi, R.B., Ashiq, M.N., Zafar, Z.I., Mater. Res. Bull. 48, 4775-4779 (2013); https://doi.org/10.1016/j.materresbull.2013.08.021

[22] Gul, I., Ahmed, W., Maqsood, A., J. Magn. Magn. Mater. 320, 270-275 (2008); https://doi.org/10.1016/j.jmmm.2007.05.032

[23] E. AlArfaj, S. Hcini, A. Mallah, M.H. Dhaou, M.L. Bouazizi, J. Supercond. Nov. Magn. 31 (2018) 4107-4116; https://doi.org/10.1007/s10948-018-4694-8

[24] M.A. Dar, V. Verma, S. Gairola, W. Siddiqui, R.K. Singh, R. Kotnala, Appl. Surf. Sci. 258 (2012) 5342-5347; https://doi.org/10.1016/j.apsusc.2012.01.158

[25] M. Zulqarnain, S. Ali, U. Hira, J. Feng, M. Khan, M. Rizwan, K. Javed, G. Farid, M. Hasan, J. Alloy. Compd. 894 (2022) 162431; https://doi.org/10.1016/j.jallcom.2021.162431

[26] Maxwell, J.C., Electricity and magnetism, Dover New York (1954)

[27] V. Ganeshchandra Prabhu, A.R. Paloly, N.G. Divya, M. Junaid Bushiri, Materials Science & Engineering B 228 (2018) 132-141; https://doi.org/10.1016/j.mseb.2017.11.017

[28] Senbeto, E. K., Elangovan, S. (2023), Journal of Nanomaterials, 2023; https://doi.org/10.1155/2023/5103278

[29] A.A. Al-Ghamdi, F. Al-Hazmi, R.M. Al-Tuwirqi, F. Alnowaiser, O.A. Al-Hartomy, F. El-Tantawyd, F. Yakuphanoglu, Solid State Sci. 19 (2013) 111-116; https://doi.org/10.1016/j.solidstatesciences.2013.02.005